Quantum transport in indium nitride nanowires

Liubing Huang, Dongdong Li, Paichun Chang, Sheng Chu, Hans Bozler, Igor S. Beloborodov, and Jia G. Lu

Phys. Rev. B **83**, 245310 — Published 21 June 2011

DOI: 10.1103/PhysRevB.83.245310

Quantum Transport in Indium Nitride Nanowires

Liubing Huang, [†] *Dongdong Li,* [†] *Igor. S. Beloborodov,* [§] *and Jia G. Lu* *[†]

† Department of Physics and Department of Electrical Engineering, University of Southern California, Los Angeles, California 90089-0484, USA.

§ Department of Physics & Astronomy, California State University, Northridge, California 91330, USA.

[*] To whom correspondence should be addressed. Email: jia.grace.lu@usc.edu.

TABLE OF CONTENT GRAPHIC

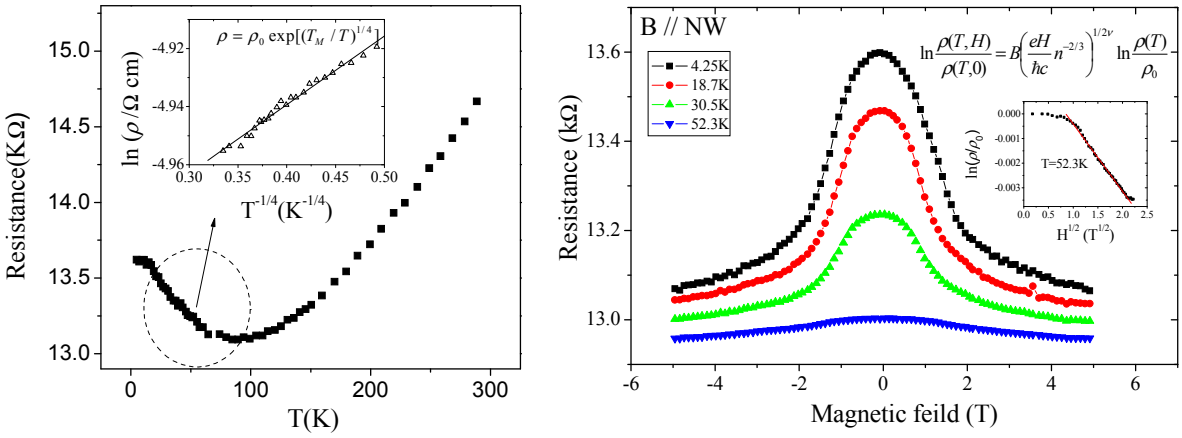

ABSTRACT

Transport measurements are performed under the variations of temperature and magnetic field on single crystalline InN nanowires. Conduction at low temperature reveals 3D Mott variable range hopping mechanism. With rising temperature, an semiconductor-to-metal transition is observed around 80 K. In addition, the nanowire exhibits negative magnetoresistance under both parallel and perpendicular fields, due to the suppression of the electron wavefunction interference. A field direction asymmetry on the change of magnetoresistance is examined, attributing to the conduction channel anisotropy.

Key Words: InN nanowire, quantum transport, variable range hopping, negative magnetoresistance

Charge transport properties of low dimensional systems are of profound interest due to the quantum mechanical phenomena that occur when their sizes reduce to nanometer scales.[1-3] Advance in nanofabrication has opened the pathway to probe the fundamental properties manifested in such strongly confined systems. Among them, quasi-one-dimensional (quasi-1D) materials (*e.g.* nanowires and nanotubes) synthesized via bottom-up technology with highly crystalline structures and highly anisotropic geometries are excellent candidates for understanding quantum transport properties and for developing potential nanoelectronic devices.[2, 4-7] Among the semiconductor nanowires, indium-based III-V semiconductors, such as InN, InAs and InSb, are known to have high conductivity and extremely high electron mobility.[8-13] Thus, it is of significant interest to investigate their quantum transport properties in order to evaluate them as the future building blocks for high-speed electronic devices.

InN nanowires are synthesized by a low-pressure chemical vapor deposition (CVD) method. The source InN powder is placed in an alumina boat at the center of a horizontal tube furnace, where the temperature is elevated to 580 °C in 10 min under continuous ammonia (NH_3) flow at 50 sccm in a controlled pressure of 1 torr. Silicon substrate coated with 10 nm Au catalyst film is placed close to the source powder. Figure 1a shows a scanning electron microscope (SEM) image of InN nanowires with diameter ranging from 50 to 200 nm. The stoichiometry of the as-grown InN nanowires is investigated by energy dispersive X-ray spectroscopy (EDS) analysis. As shown in the inset of Figure 1a, distinct indium (In) and nitrogen (N) peaks confirm the elemental composition, while the silicon (Si) peak originates from the substrate. The atomic ratio of In:N is close to 1:1, suggesting good stoichiometry of the InN nanowires. Crystal structure of the nanowires is examined by X-ray diffraction (XRD) pattern as plotted in Figure 1b. All diffraction peaks match well with those of the standard wurtzite structure InN (JCPDS file No. 50-1239). TEM image of a single InN nanowire demonstrating high aspect ratio structure is shown in Figure 1c. High-resolution transmission electron microscopy (HRTEM image in Fig.1d) analysis is also performed to further examine the crystal structure. It displays a single crystalline system with pure close-packed wurtzite structure. The nanowire grows along [100] direction and the interplanar spacing of the (100) planes is estimated to be 0.307 nm, which matches that of InN single

crystal with a lattice constant a= 0.354 nm.[14] The Fast Fourier Transform (FFT) result (inset in Fig.1d) shows typical diffraction pattern of the hexagonal system at the [001] projection direction.

The InN nanowires suspended in solution are then dispersed onto a Si/SiO_2 substrate for subsequent contact electrode patterning. Photolithography followed by metallization of Pd/Au is processed to define four-probe contacts with equal spacing (as depicted in Fig 2a inset). Palladium (Pd) is selected as the adhesive contact metal to form ohmic electrical contacts because its work function (5.12-5.65 eV)[15, 16] matches with the large electron affinity of InN (5.8 eV).[17, 18]

Figure 2a shows the resistance change of an individual InN nanowire (diameter ~117 nm) in the measurement temperature range of 5 - 300k. First, one observes in the temperature range from 15 to 80 K, the resistance decreases monotonically with temperature rising from 15 to 80 K, namely an insulating characteristic. The conduction at this range of temperature is governed by variable range hopping mechanism. Next, a distinct semiconductor-to-metal transition is observed around 80 K. Above this transition temperature, enhanced scatterings due to Coulomb interactions play a dominant role, giving rise to a metallic-like characteristic. This transition has been reported in other semiconducting nanowires.[19]

There have been previous transport measurements on InN nanowire showing metallic behavior[20] at low temperature range, indicating the formation of an accumulation layer. The origin of its existence is not yet clear.[20-26] In contrast, *n*-type semiconducting behavior[27] has also been demonstrated. Likewise in our work, a semiconductor-to-metal transition is observed, suggesting that the Fermi level is situated at the donor states below the conduction band edge E_c. Under this context, electrons localized close to the Femi level conduct via hopping at low temperatures from one localized state to the other. The InN nanowire presented here has a diameter of 117 nm, much larger than the Bohr radius (~4.6 nm)[28, 29], so that the electron transport reveals bulk 3D conduction.

To understand quantitatively the hopping transport mechanism, we will focus on the hopping regime for nanowire system with diameter D satisfying the inequality:

$$D >> r_{hop}(T) >> a_B \quad (1)$$

where $r_{hop}(T) = \xi_0 (T_0 / T)^{\beta}$ is the electron hopping length, with β being the numerical constant discussed below in equation (2); ξ_0 is the localization length deep in the insulating regime. $\xi_0 \sim a_B$, where a_B is the Bohr radius; and T_0 is the characteristic temperature scale discussed below in equation (3). When this inequality Eq. (1) is satisfied, the wire can be considered as a 3D system[30]. At low temperatures, the typical hopping distance $r_{hop} \sim 10\xi_0$, so that the hopping conduction (*i.e.* Eq. (1)) is easy to satisfy. And the temperature dependent resistivity can be expressed as[33]

$$\rho = \rho_0 \exp[(T_0 / T)^{\beta}] \quad (2)$$

where the power β depends on different hopping conductivity mechanisms: $\beta = 1/2$ at very low temperature (Efros-Shklovskii varible range hopping (ES VRH) regime), $\beta = 1/(1+d)$ at relatively higher temperature (Mott VRH regime) where d is the dimensionality; and $\beta = 1$ at even higher temperature (nearest neighbor hopping (NNH) regime). To clarify the hopping mechanism, the crossover temperature between ES to Mott VRH is first considered. The crossover temperature is given by:

$$T_{cross} = T_M (\frac{T_{ES}}{T_M})^{(d+1)/(d-1)} \quad (3)$$

where T_{M} and T_{ES} are the characteristic temperature scales depending on the localization length and the density of states υ_0 at the Fermi level,[31, 32, 33] $T_M = \frac{1}{\nu_0 \xi_0^d}$ is the characteristic temperature in the Mott VRH model. And $T_{ES} = \frac{e^2}{4\pi\varepsilon\varepsilon_0\xi_0}$ is the characteristic temperature in the ES VRH model. Taking *d=3* gives the crossover temperature $T_{cross} = {T_{ES}}^2 / T_M < 5K$, which is below the temperature range in our experiment. Next, to distinguish Mott VRH from the nearest neighbor hopping, we plot $\ln(\rho)$ versus T^{-1}, which is not a straight line, so the NN hopping can be easily ruled out. Thus Mott VRH model is valid in our InN nanowires. Figure 2b plots $\ln(\rho)$ versus $T^{-1/4}$ at low temperature range (17 - 80 K), fitting

well with a linear expression. This fitting confirms Mott VRH hopping model, and shows that the electron conduction through the nanochannel follows bulk 3D hopping transport model. Therefore, the temperature dependent resistivity can be written as:

$$\rho = \rho_0 \exp[(T_M / T)^{1/4}] \qquad (4)$$

To further explore the transport mechanisms of the electrons at low temperature, magneto-resistance (MR) measurements are carried out by applying external magnetic fields ranging from -5 to 5 T at temperatures from 4.2 to 58 K, which is in the vicinity of semiconductor-to-metal transition temperature in terms of the phonon energy. Figures 3a and b show the MR data with the magnetic field perpendicular and parallel to the nanowire long axis, respectively, both exhibiting negative MR (*i.e.* resistances decrease with increasing magnetic field)[33]. The negative MR effect becomes less pronounced with increasing temperature due to shorter hopping distance, $r_{hop}(T) = \xi_0 \sqrt[4]{T_M / T}$. From Figs. 3a and b, we observe that the rate change of MR in field parallel to the nanowire long axis is higher, *i.e.* the resistance change is much stronger in parallel field than in perpendicular field.

The negative magnetoresistance phenomenon measured in InN nanowires in the vicinity of semiconductor-to-metal transition can be analyzed using the VRH model, which is consistent with the temperature dependent conduction at zero field described earlier. The magnetic field produces two effects: i) classical and ii) quantum. The classical effect is squeezing the electron wave functions [34]. This mechanism leads to the positive magnetoresitance, *i.e.* the larger the magnetic field the larger the sample resistance. However, in addition to the classical mechanism, there is a second mechanism leading to the negative MR observed. This mechanism has a quantum mechanical origin and is related to the fact that different electron wave functions can interfere with each other during the electron hopping process. The magnetic field destroys this interference thus leading to the negative magnetoresistance. The negative magnetoresistance is well known in the theory of weak localization[35]. However, this theory assumes that all electronic states are delocalized, thus it is not directly applicable to our samples. On the contrary, as follows from our resistance measurement at zero magnetic field, all electronic states in the nanowire

channels are localized. This is why we have used VRH mechanism (Eq. (4)) to analyze the data. And in the VRH regime, the interference between different electron wave functions still exists. A magnetic field H strongly affects the interference if the magnetic flux through a typical closed trajectory S is comparable to the quantum flux $\Phi_0 = \frac{\pi\hbar c}{e}$. The typical closed trajectory is defined as $S \sim kn^{-2/3}$, where n is the impurity concentration, and $k \sim \xi n^{\frac{1}{3}}\left(\frac{T_M}{T}\right)^{\frac{1}{4}}$ is the average number of hops within the phase coherence time $\tau_\phi \sim \exp\left(\frac{T_M}{T}\right)^{\frac{1}{4}}$ over which the electron makes a transition into a quantum state that is incoherent with respect to the initial state. Thus the negative magnetoresistance is applicable for magnetic field satisfying the condition: $\frac{eH}{\hbar c}\left(\frac{T_M}{T}\right)^{\frac{1}{4}} \xi n^{-\frac{1}{3}} >> 1$.

Based on the VRH model we discussed earlier, we assume that the inequality Eq. (1) is still valid in the vicinity of the semiconductor-to-metal transition, although in this regime, this inequality may be more difficult to satisfy since the localization length ξ can be rather large

$$\xi = \frac{\xi_0}{(1 - n/n_c)^{\nu}} >> a_B \tag{5}$$

where $\xi_0 \sim a_B$ is the localization length deep in the insulation regime and $0 < \nu < 1$ is the critical index. n and n_c denote the impurity concentration and the critical impurity concentration. It is known that n_c depends on the magnetic field in the following way [36]

$$\frac{n_c(H) - n_c(0)}{n_c(0)} = A\left(\frac{eH}{\hbar c} n_C(0)^{-2/3}\right)^{1/2\nu} \tag{6}$$

where A is a numerical constant. In the high field regime, $A < 0$, $n_c(H) < n_c(0)$ leads to $\xi(H) - \xi(0) > 0$. In the Mott VRH regime, the resistance is given by Eq. (4). The temperature scale T_M depends on the localization length ξ as $T_M \sim \xi^{-d} = \xi^{-3}$ with *d=3* as discussed earlier. Using the fact that

in the vicinity of semiconductor-to-metal transition, the parameter $\frac{n_c(0)-n_c(H)}{n_c(0)} << 1$, and expanding Eq. (4) yields an expression:

$$\ln\frac{\rho(T,H)}{\rho(T,0)} = B\left(\frac{eH}{\hbar c}n^{-2/3}\right)^{1/2\nu}\ln\frac{\rho(T)}{\rho_0} \qquad (7)$$

where $B=\frac{3}{4}A\nu$ is a numerical coefficient[37]. The temperature dependence of $\ln[\rho(T,H)/\rho(T,0)]$ is given by the factor $\ln[\rho(T)/\rho_0]$, and can be measured independently as has been shown in the zero field resistivity measurement. And the magnetic field dependent of the $\ln[\rho(T,H)/\rho(T,0)]$ at constant temperature has a linear expression with respect to $H^{1/(2\nu)}$. Fig 3c shows the plot of this magnetoresistivity ratio, with the best fit obtained for $\nu=1$.

Finally we explore the MR dependence on the applied field direction. Figure S1 in the supplemental information shows logarithm plots of normalized resistivity versus $H^{1/2}$ with the magnetic field perpendicular and parallel to the. nanowire axis, depicting a much stronger effect when the field is in the parallel direction. The origin of this direction asymmetry lies in the fact that the nanowire conduction channel is strongly anisotropic. So the shift in the threshold, Eq. (6) depends on the angles between the direction of magnetic field H and the axes of the ellipsoid of the diffusion coefficient D_{ij}.[38] The magnetic field in this case transforms into $\widetilde{H}=H\left(\frac{D_1}{D_2}\right)$, where $D_1=\sqrt{D_\perp(D_\perp\cos^2\theta+D_{//}\sin^2\theta)}$, $D_2=\sqrt[3]{D_{//}D_\perp^2}$, with θ being the angle between H and the wire long axe[38]. Then in this anisotropic scenario, a concentration threshold n_C and its shift are defined by Eq. (6) with magnetic field H replaced by $\widetilde{H}$, that leads to the displacement of the threshold depending on the angle θ. Therefore, in parallel field when $\theta=0$, $D_1=D_\perp$ and as a result for magnetic field, we obtain $\widetilde{H}=H\left(\frac{D_\perp}{D_{//}}\right)^{1/3}$. In a

perpendicular magnetic field when $\theta = \pi/2$ and $D_1 = \sqrt{D_\perp D_{//}}$, we get $\widetilde{H} = H\left(\frac{D_{//}}{D_\perp}\right)^{1/6}$. Thus one obtains the following result for the magnetoresistance ratio for the perpendicular and parallel magnetic fields, showing the anisotropic effect of the applied field direction.

$$\frac{\ln[\rho(T,H,\theta=\pi/2)/\rho(T,0)]}{\ln[\rho(T,H,\theta=0)/\rho(T,0)]} = \left(\frac{D_{//}}{D_\perp}\right)^{1/4\nu} \qquad (8)$$

In summary, InN nanowires have been successfully synthesized using catalytic CVD method, showing single crystalline structure in wurtzite phase as confirmed by XRD and HRTEM. To investigate the fundamental transport mechanisms of through nanowire, four probe transport measurements on individual InN nanowire are performed with respect to temperature and magnetic field. A clear semiconductor-to-metal transition at T ~ 80 K is revealed. Below the transition, the conduction is dominated by 3D Mott variable range hopping. In addition, a negative magneto-resistance is observed due to the destruction of the interference of the electron wavefunctions as magnetic field increases. Asymmetry of the MR effect in parallel and perpendicular fields is investigated, showing that the MR change is much stronger in wire axis-parallel field due to the anisotropy in the conduction channel.

ACKNOWLEDGMENT

The authors thank Chu Sheng for experimental measurements and Paichun Chang for manuscript support. We are also indebted to Prof. Ruqian Wu for helpful discussions. D.L. is grateful for the support from Science & Technology Commission of Shanghai Municipality (China, grant number: 10DZ1210300). D.L. current address is Division of Energy and Environmental Research, Shanghai Advanced Research Institute, Chinese Academy of Sciences, Shanghai 201203 (China).

REFERENCES

[1] H. Park, J. Park, A. K. L. Lim, E. H. Anderson, A. P. Alivisatos, and P. L. McEuen, Nature **407**, 57 (2000).

[2] J. G. Lu, P. C. Chang, and Z. Y. Fan, Mater. Sci. Eng. R. **52**, 49 (2006).

[3] H. Luth, et al., physica status solidi (c) **7**, 386.

[4] Y. Cui, Z. H. Zhong, D. L. Wang, W. U. Wang, and C. M. Lieber, Nano Lett **3**, 149 (2003).

[5] R. S. Thompson, D. D. Li, C. M. Witte, and J. G. Lu, Nano Lett **9**, 3991 (2009).

[6] L. T. Tsai, S. P. Chiu, J. G. Lu, and J. J. Lin, Nanotechnology **21** (2010).

[7] F. Qian, Y. Li, S. Gradecak, D. L. Wang, C. J. Barrelet, and C. M. Lieber, Nano Lett **4**, 1975 (2004).

[8] Y. Li, J. Xiang, F. Qian, S. Gradecak, Y. Wu, H. Yan, H. Yan, D. A. Blom, and C. M. Lieber, Nano Lett **6**, 1468 (2006).

[9] E. Cimpoiasu, E. Stern, G. S. Cheng, R. Munden, A. Sanders, and M. A. Reed, Braz J Phys **36**, 824 (2006).

[10] T. Richter, C. Blomers, H. Luth, R. Calarco, M. Indlekofer, M. Marso, and T. Schapers, Nano Lett **8**, 2834 (2008).

[11] C. Y. Chang, G. C. Chi, W. M. Wang, L. C. Chen, K. H. Chen, F. Ren, and S. J. Pearton, Applied Physics Letters **87**, 093112 (2005).

[12] C. Y. Chang, G. C. Chi, W. M. Wang, L. C. Chen, K. H. Chen, F. Ren, and S. J. Pearton, Journal of Electronic Materials **35**, 738 (2006).

[13] P. D. C. King, T. D. Veal, and C. F. McConville, Journal of Physics: Condensed Matter **21** (2009).

[14] M. S. Hu, G. M. Hsu, K. H. Chen, C. J. Yu, H. C. Hsu, L. C. Chen, J. S. Hwang, L. S. Hong, and Y. F. Chen, Applied Physics Letters **90**, 123109 (2007).

[15] H. B. Michaelson, Journal of Applied Physics **48**, 4729 (1977).

[16] D. F. Gu, S. K. Dey, and P. Majhi, Applied Physics Letters **89**, 082907 (2006).

[17] S. X. Li, et al., Physical Review B **71**, 161201(R) (2005).

[18] J. W. Ager, N. Miller, R. E. Jones, K. M. Yu, J. Wu, W. J. Schaff, and W. Walukiewicz, Physica Status Solidi B-Basic Solid State Physics **245**, 873 (2008).

[19] P. C. Chang and J. G. Lu, Appl. Phys. Lett. **92**, 212113 (2008).

[20] T. Richter, H. Luth, T. Schapers, R. Meijers, K. Jeganathan, S. E. Hernandez, R. Calarco, and M. Marso, Nanotechnology **20**, 405206 (2009).

[21] F. Werner, F. Limbach, M. Carsten, C. Denker, J. Malindretos, and A. Rizzi, Nano Lett **9**, 1567 (2009).

[22] D. Segev and C. G. Van de Walle, Europhys Lett **76**, 305 (2006).

[23] H. Lu, W. J. Schaff, L. F. Eastman, and C. E. Stutz, Applied Physics Letters **82**, 1736 (2003).

[24] T. D. Veal, I. Mahboob, L. F. J. Piper, C. F. McConville, H. Lu, and W. J. Schaff, Journal of Vacuum Science & Technology B **22**, 2175 (2004).

[25] K. A. Rickert, A. B. Ellis, F. J. Himpsel, H. Lu, W. Schaff, J. M. Redwing, F. Dwikusuma, and T. F. Kuech, Applied Physics Letters **82**, 3254 (2003).

[26] I. Mahboob, T. D. Veal, C. F. McConville, H. Lu, and W. J. Schaff, Physical Review Letters **92**, 036804 (2004).

[27] S. Lee, W. Lee, K. Seo, J. Kim, S. H. Han, and B. Kim, Nanotechnology **19**, 415202 (2008).

[28] H. Lu, W. J. Schaff, L. F. Eastman, J. Wu, W. Walukiewicz, D. C. Look, and R. J. Molnar, Mater. Res. Soc. Symp. Proc. **743**, L4.10.1. (2003).

[29] A. Chaudhry and M. S. Islam, Journal of Nanoscience and Nanotechnology **8**, 222 (2008).

[30] For thinner nanowires with diameter D < r_hop the nanowire is effectively 1D system therefore the electron transport is defined by the weakest link leading to activation resistivity behavior.
[31] S. Adachi, *Handbook of Physical Properties of Semiconductors* (Kluwer, Dordecht, 2004).
[32] Y. F. Lin, W. B. Jian, C. P. Wang, Y. W. Suen, Z. Y. Wu, F. R. Chen, J. J. Kai, and J. J. Lin, Applied Physics Letters **90**, 223117 (2007).
[33] Note that the measurements in perpendicular and parallel fields are done on two different samples. They are synthesized in the same run, but show slightly different resistances.
[34] B. I. ShklovskiI and A. L. Efr eds., *Electronic properties of doped semiconductors* (Springer, New York, 1984).
[35] D. E. Khmel'nitskii, Physica B+C **126**, 235 (1984).
[36] D. E. Khmel'nitskii and A. I. Larkin, Solid State Communications **39**, 1069 (1981).
[37] B. L. Altshuler, A. G. Aronov, and D. E. Khmelniskii, JETP letters **36**, 195 (1982).
[38] B. L. Altshuler, A. G. Aronov, A. I. Larkin, and D. E. Khmelnitskii, Sov. Phys. JETP **54**, 411 (1981).

FIGURE CAPTIONS

Figure 1. (a) SEM image shows large quantity of InN nanowires grown on Si substrate. Inset: EDS spectrum of the as-grown InN nanowires exhibits 1:1 stoichiometry. (b) XRD pattern indexed to wurtzite InN. (c) TEM image of a single InN nanowire shows high aspect ratio structure. (d) HRTEM image shows single crystalline wurtzite structure with inter-plane distance ~0.307 nm, indicating the stacking direction along [100]. Inset: corresponding FFT pattern of a hexagonal system.

Figure 2. (a) Temperature dependent resistance measurement of a single InN nanowire contacted by four probes (Inset shows the SEM image of the device). Scale bar is 5 μm. (b) $\ln \rho$ versus $T^{-1/4}$ at the temperature range of 17 - 80 K, showing a linear fitting to 3D Mott VRH model.

Figure 3. Magneto-resistance (MR) measurement with the magnetic field applied (a) perpendicular and (b) parallel to the nanowire long axis at different temperatures. (c) Linear fitting of $\ln[\rho(T,H)/\rho(T,0)]$ versus $H^{1/2}$ under parallel magnetic field.

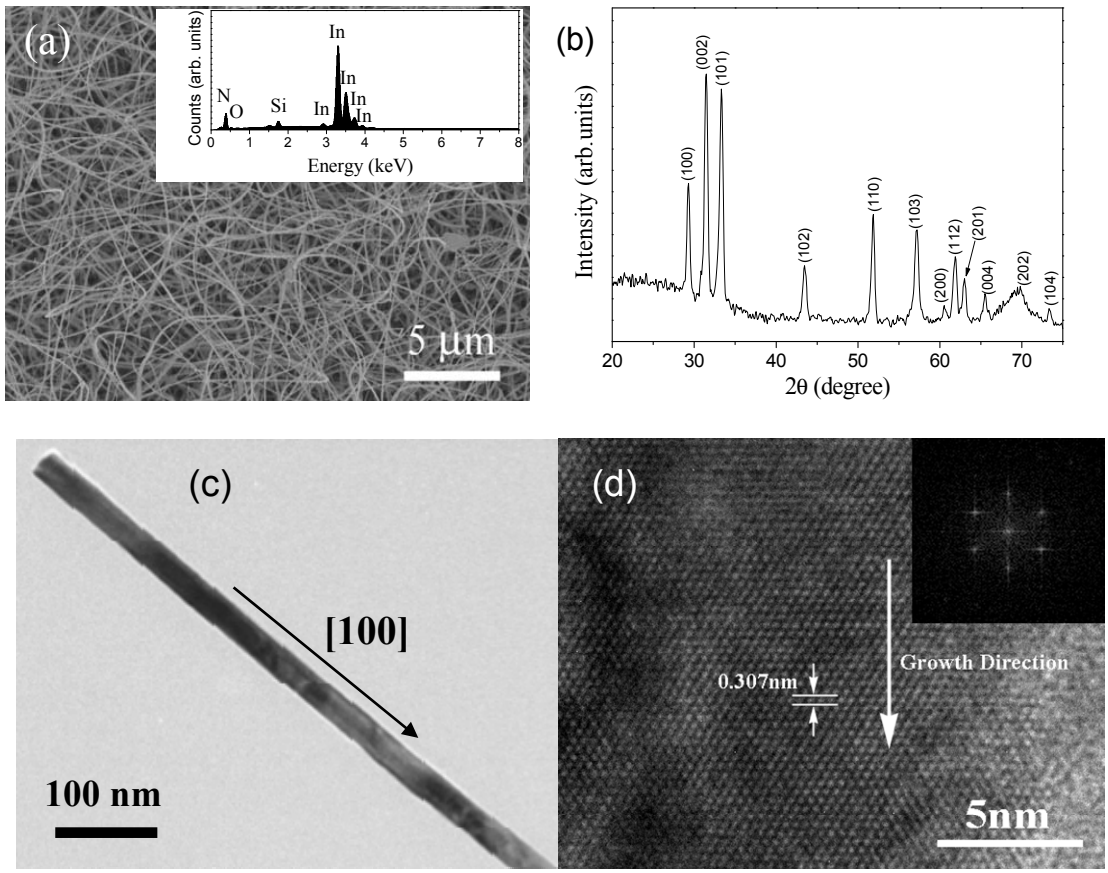

Figure 1

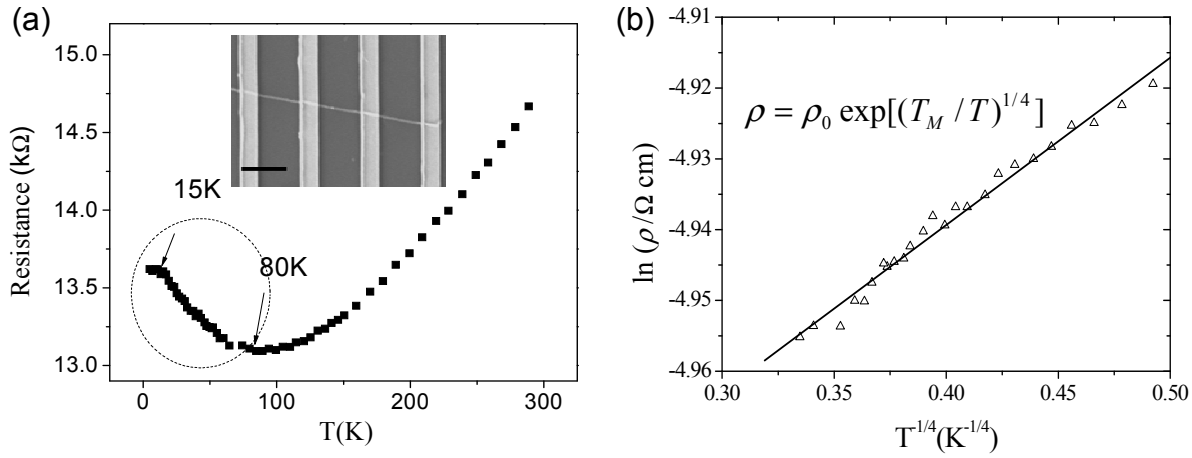

Figure 2

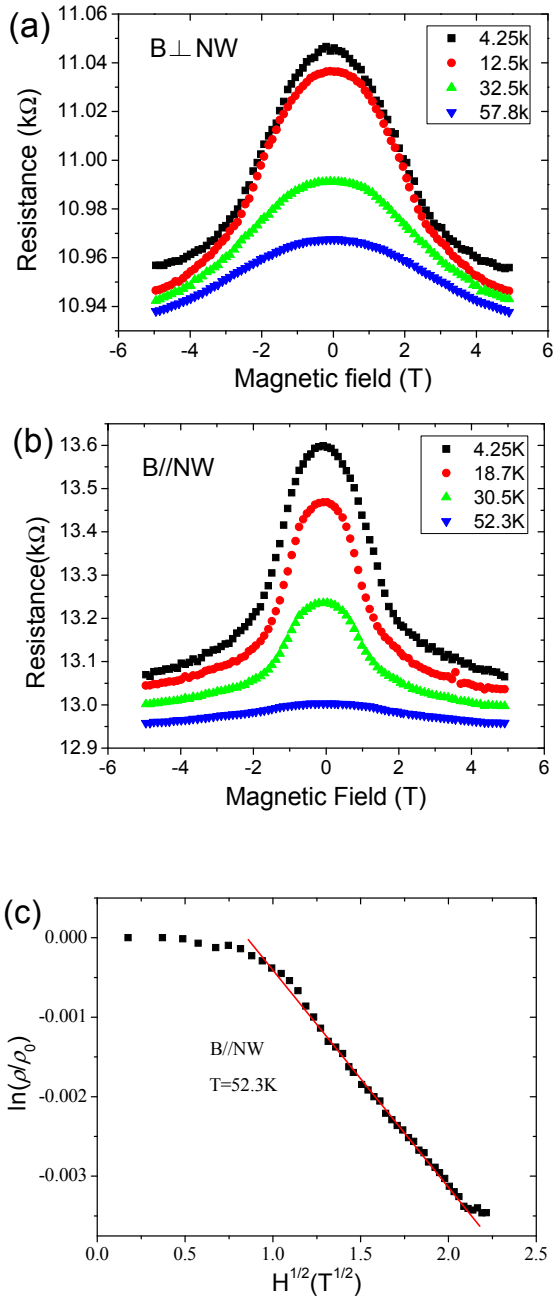
(a)
B⊥NW
4.25k
12.5k
32.5k
57.8k
Resistance (kΩ)
Magnetic field (T)
(b)
B//NW
4.25K
18.7K
30.5K
52.3K
Resistance(kΩ)
Magnetic Field (T)
(c)
B//NW
T=52.3K
ln(ρ/ρ0)
H1/2(T1/2)

Figure 3